Highly Stretchable and Rehealable Wearable Strain Sensor Based on Dynamic Covalent Thermoset and Liquid Metal

Chuanqian Shi[1,2,†], Ying Zhao[1,†] Pengcheng Zhu[2,3] Jianliang Xiao[2,*] and Guohua Nie[1,*]

[1] School of Aerospace Engineering and Applied Mechanics, Tongji University, Shanghai 200092, China
[2] Department of Mechanical Engineering, University of Colorado Boulder, Boulder, Colorado 80309, USA
[3] School of Physics and Microelectronics, Zhengzhou University, Zhengzhou 450001, China.
† These authors contributed equally.
E-mail: ghnie@tongji.edu.cn (G.H. Nie), Jianliang.Xiao@colorado.edu (J. Xiao)

Received xxxxxx
Accepted for publication xxxxxx
Published xxxxxx

Abstract

Cutting-edge technologies of wearable electronics have recently attracted tremendous attention. One of the key issues lies in the choice of compliant and environmental-friendly materials and cost-effective fabrication methods. We here report a rehealable and highly stretchable wearable strain sensing system enabled by advanced materials. By embedding patterned liquid metal (LM) line traces into dynamic covalent thermoset polyimine through a low-cost fabrication method, a mechanically flexible and electrically sensitive strain sensor is obtained. We proposed an analytical model based on length fractions of the strain sensor to describe the resistance change under applied strain. The results show good agreement with finite element simulation and experiment. Because of the bond exchange reactions in polyimine and the flowability of LM, the sensing system has excellent rehealability when it's damaged. These superior properties make the strain sensor quantitatively precise, economically friendly and environmentally sustainable, and thus can find wide applications in various areas.

Keywords: dynamic covalent thermoset, strain sensing system, stretchability, rehealability, analytical model

1. Introduction

Soft and stretchable integrated electronic systems have gained wide popularity recently due to their superior mechanical compliance and conformability, which distinguishes them from conventional rigid electronic devices[1–6]. Cutting-edge technologies of stretchable, skin-mountable, and wearable electronics are able to effectively accommodate large strain when integrated onto soft, elastic and curved surfaces[7–11]. Ultralow modulus and high stretchability of electronic systems are achieved by designing new structural layouts[12–14] and developing novel materials[15–18]. However, stretchable conductors made of metallic materials often suffer from cycling induced fatigue, which cannot be easily improved by new structural designs[19,20].

Recently, various wearable strain sensors with high sensing range (>50%) have been developed for their broad applications in human motion detection, health care, human-machine interfaces[21–25]. Strain sensors can be classified into two types: resistive-type and capacitive-type sensors. Resistive-type sensors are typically composed of composites combining electrically conductive sensing films with flexible substrates[26–28]. When stretched, the microstructure of sensing films evolves, and the electrical resistance changes

accordingly. On the other hand, a capacitive-type sensor consists of a highly compliant dielectric layer between a pair of stretchable electrodes. When stretched, two electrodes become closer, and the capacitance increases[29]. Alternatively, stretchable and wearable strain sensors can also be classified according to their materials, into categories such as fiber, liquid metal (LM), and piezoelectricity based strain sensors[30–32]. As a liquid-state conductor, the LM features excellent electrical conductivity, fatigue-free characteristics and extremely high deformability, thus is an ideal component for wearable strain sensors[33–35].

Moreover, materials that can heal like natural skins have also been developed in wearable electronics. Self-healing or rehealing capabilities can help wearable electronics to gain benefits of reliability, durability, cost and performance. While some healing mechanisms can automatically respond to damages without stimuli[36], most materials still require moderate external stimulation—such as heat, pressure, lights and reagents—to trigger the healing process[37–40]. Various strategies have also been investigated to achieve healability, including metal-ligand supramolecular, microvascular agents, hydrogen bonds, and dynamic covalent bonds[41–45]. Among the mechanisms, dynamic covalent bonding in polymer networks is usually stronger than supramolecular interactions, thus making such materials more robust and can operate under a wider range of conditions[46]. More recently, a series of dynamic covalent thermoset polyimine that can self-heal or reheal under modest external stimuli have been developed[47–52].

Here, we present a new type of flexible, highly stretchable, and rehealable strain sensing system enabled by eutectic LM alloy and dynamic covalent thermoset polyimine. As LM is a liquid, it doesn't add rigidity and provides excellent deformability to the strain sensing system. Moreover, unlike conventional metal conductors[53,54], LM conductors doesn't experience fatigue. Furthermore, a dynamic covalent thermoset polyimine matrix is not only highly stretchable, but also rehealable from damages. To provide prediction to the strain sensing system, we have also established an analytical model based on length fractions to describe the resistance change under applied strain, which shows good agreement with finite element simulations and experimental measurements.

2. Design and Synthesis

The strain sensor system presented here incorporates dynamic covalent thermoset polyimine as both the substrate and encapsulation for LM channel (Figure 1a). The cross-

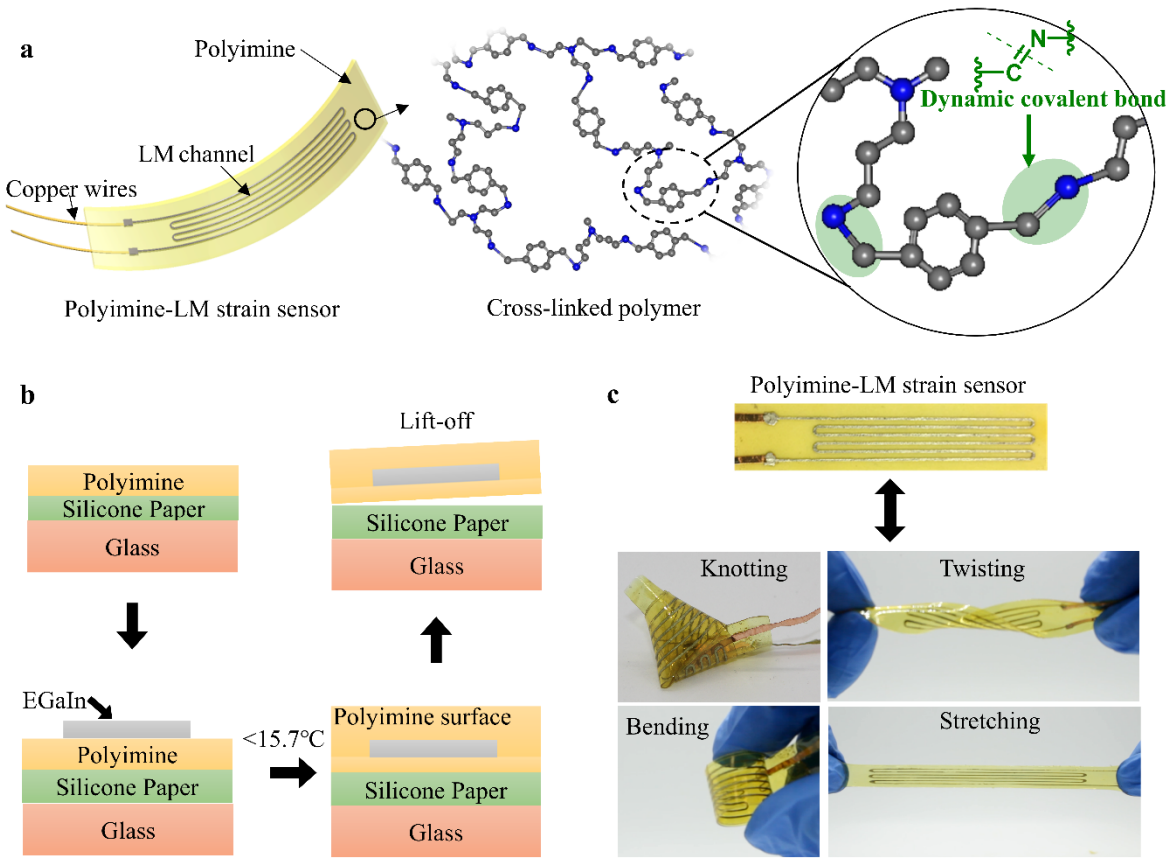

Figure 1. Design and schematic illustration of the polyimine-LM strain sensor. (a) Schematic illustration of a strain sensor based on dynamic covalent thermoset polyimine and LM. (b) Schematic illustration of the fabrication process of the strain sensor. (c) Optical images of the strain sensor being knotted, twisted, bended and stretched.

linked polyimine network (Figure 1a, left) are synthesized using three commercially available monomers: terephthalaldehyde, 3,3′-diamino-*N*-methyldipropylamine and tris(2-aminoethyl)amine (Figure S1). As show in Figures S2 and S3, the highly stretchable polyimine has low modulus ~2 MPa, which leads to a wide sensing range of the strain sensor system. The LM channel is made of eutectics Gallium-Indium (EGaIn) alloy, which maintains liquid state at room temperature (15.7°C melting point)[33]. In order to improve the strain sensitivity, the pure EGaIn was mixed with 6%wt SiO_2 microparticles (40 μm diameter, Sigma-Aldrich) at room temperature. The comparison of the strain sensitivity or gauge factor (GF) between pure LM sensor and SiO_2 doped LM sensor is exhibited in Figure S4, and the GF of the doped LM one has increased by an order of magnitude. It's worth pointing that such sensitivity is a high gauge factor in liquid based (LM, ionic glycol and link) strain sensors[30,55-57]. The fabrication process of the polyimine-LM strain sensor is schematically illustrated in Figure 1b. It started with curing a synthesized polyimine film onto a silicone paper glued on a glass slide (Figure 1b, top left). The SiO_2 doped LM (Figure S5a) has the viscosity while maintaining the fluidity, which improves the printability, so that the mixed LM can be easily brushed onto the weak adhering polyimine film against a mask at room temperature (Figure S5b). Peeling off of the mask below LM melting point 15.7 ℃ leaves patterned solid LM traces on the polyimine substrate. Then applying and curing polyimine solution on the device provided encapsulation of the LM channel. To connect the device to the external data acquisition equipment, two copper wires were embedded in the polyimine. Such fabrication process is inexpensive, scalable, and compatible with printing technology. Since the doped LM channel in the strain sensor system doesn't add any rigidity to the device and provides a combination of excellent electrical conductivity (1.1×10^6 S/m) and superior mechanical softness and stretchability, the device can be knotted (Figure 1c, top left), twisted (Figure 1c, top right), bended (Figure 1c, bottom left) and stretched (Figure 1c, bottom right).

3. Theoretical Modelling of Strain Sensor

To investigate the fractional change of resistance of the polyimine-LM strain sensor during stretching, the tensile tests of a single-line strain sensor were firstly performed (Figures 2a and S6). Kapton tapes (DuPont de Nemours, Inc.) were wrapped around the edges of the LM channel to protect the connection between the LM and the copper foil, which provides constraints on both ends during the experiment. An analytical model based on the length fractions of the strain sensor was used to describe the resistance change, which considers the effect of load and boundary condition on the resistance change under applied strain.

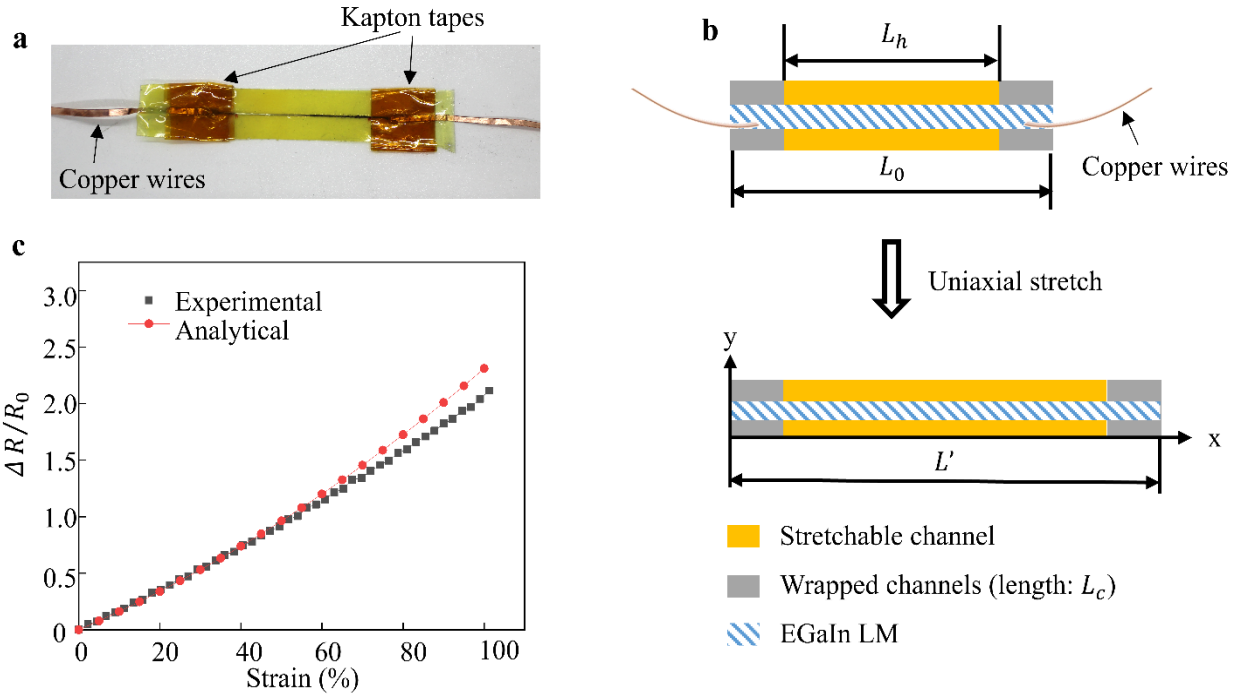

Figure 2. Analytical and experimental studies of the stretching behavior of the single-line polyimine-LM strain sensor. (a) Optical image of a single-line strain sensor. (b) Schematic illustration of the geometrical deformation of a single-line strain sensor before and after stretching. (c) Comparison of the fractional change of resistance between experimental and analytical results of a single-line strain sensor under stretching.

Figure 2b shows schematic illustration of the single-line polyimine-LM strain sensor under stretching. The initial length and cross-sectional area of the sensor are denoted by L_0 and A_0, respectively. The initial resistance of a strain sensor (R_0) is expressed as

$$R_0 = \rho \frac{L_0}{A_0}, \quad (1)$$

where ρ is the electrical resistivity of the LM. As shown in Figure 2b, the strain sensor is divided into a horizontally stretchable channel and channels wrapped by Kapton tapes that cannot deform on both ends. We define the length of the stretchable channel as L_h and the total length of the wrapped channels as L_c, and $L_0 = L_h + L_c$. We also define a and c as their length fractions by $a = L_h / L_0$, $c = L_c / L_0$, which naturally yields $a + c = 1$.

Under uniaxial tension along x direction, the deformation gradient of the sensor is expressed as

$$\mathbf{F} = \begin{bmatrix} \lambda_1 & & \\ & \lambda_2 & \\ & & \lambda_3 \end{bmatrix}, \quad (2)$$

where λ_1, λ_2, and λ_3 are stretches along x, y and z directions, respectively. Since the materials of the sensor are isotropic, we have $\lambda_2 = \lambda_3$. Assuming the LM and polyimine as incompressible materials, which gives $\det(\mathbf{F}) = \lambda_1\lambda_2\lambda_3 = 1$, and $\lambda_2 = \lambda_1^{-1/2}$. Therefore, the length of the stretched channel becomes

$$L' = L_h' + L_c' = \lambda_1 L_h + L_c, \quad (3)$$

and the cross-section area after stretching is

$$A' = \lambda_2^2 A_0. \quad (4)$$

If we assume the device deforms uniformly, λ_1, λ_2 and λ_3 are constants, and can be expressed by the engineering strain ε and Poisson's ratio υ as

$$\lambda_1 = 1 + \varepsilon, \quad (5)$$

$$\lambda_2 = 1 - \upsilon\varepsilon. \quad (6)$$

The total resistance of a single-line polyimine-LM strain sensor consists of the stretchable channel and the wrapped channels,

$$R^{\text{Single-line}} = R_h + R_c, \quad (7)$$

where R_h is the resistance of stretchable channel after stretching, and R_c is the resistance of wrapped channel which remains constant due to constraints of Kapton tapes. Combining Equation (1), (3) and (4), the resistance of stretchable channel after stretching is

$$R_h = \frac{\rho L_h'}{A'} = \frac{\rho \lambda_1^2}{A_0} L_h, \quad (8)$$

and the electrical resistance of strain sensor in terms of length fractions is

$$R^{\text{Single-line}} = \frac{\rho\lambda_1^2}{A_0} a L_0 + \frac{\rho}{A_0} c L_0 = (a\lambda_1^2 + c) R_0. \quad (9)$$

Substitute Equation (5) into Equation (9), the fractional change in resistance of a single-line polyimine-LM strain sensor is

$$\frac{\Delta R^{\text{Single-line}}}{R_0} = a(\varepsilon^2 + 2\varepsilon). \quad (10)$$

The experimental and analytical results of fractional change in resistance are shown in Figure 2c. In experiment, the total length of the channel is 40 mm and the stretchable part is 30.8 mm long (Figure 2a), which yields $a = 0.77$. Figure 2c shows that the analytical results agree well with the experimental results up to 100% strain.

In order to improve measurement accuracy and to enable the measurement of multi-directional deformation, the strain sensor channels are usually designed in the shape of a serpentine (Figure 1a and 3a). Figure 3a (top) shows an as-fabricated, undeformed serpentine polyimine-LM strain sensor. Tensile tests were performed to investigate the electrical resistance change of the serpentine polyimine-LM strain sensor. Similar to the composition of the resistance in Equation (7) of the single-line strain sensor, the resistance of a serpentine strain sensor is composed of three parts

$$R^{\text{Serpentine}} = R_h + R_v + R_c \quad (11)$$

where R_h is the resistance of the horizontal channels parallel to the stretching direction, R_v is the resistance of the semicircular channels approximately perpendicular to the stretching direction, and R_c is the resistance of the wrapped channels which remain constant.

Optical images of the device under 40%, 80% and 100% strains are shown in Figure3a. As the horizontal channels become longer, the vertical channels get wider. For the horizontal channels and wrapped channels, the electrical resistance $R_h + R_c$ would be the same expression as Equation (9), which is $R_h + R_c = (a\lambda_1^2 + c)R_0$.

Each vertical semicircular channel is approximated to a rectangle with a length equal to the semicircle perimeter and a width equal to the channel thickness. The total electrical resistance of vertical channels is $R_v = \frac{\rho}{A_0}\frac{\lambda_2}{\lambda_1\lambda_3}bL_0$, science $\lambda_2 = \lambda_3$, the expression can be given by

$$R_v = \frac{\rho}{A_0}\frac{1}{\lambda_1}bL_0 = \frac{b}{1+\varepsilon}\frac{\rho L_0}{A_0}, \qquad (12)$$

where b is the length fraction of the semicircular channels to the total length.

Substituting Equation (9) and (12) into Equation (11), we obtain the expression of the electrical resistance of a serpentine strain sensor

$$R^{\text{Serpentine}} = \frac{\rho L_0}{A_0}\left[(1+\varepsilon)^2 a + \frac{1}{1+\varepsilon}b + c\right]. \qquad (13)$$

$$\frac{\Delta R^{\text{Serpentine}}}{R_0} = (1+\varepsilon)^2 a + \frac{1}{1+\varepsilon}b + c - 1. \qquad (14)$$

As shown in Figure3a, the initial length of the sensing device and the serpentine channel are 40 mm and 266 mm, respectively. And the length proportion yields $a = 0.87$, $b = 0.07$, $c = 0.06$, respectively. For the sake of convenience, without causing confusions, the superscripts of ΔR in Equation (10) and (14) are omitted in Figure 2-5.

As a validation, we also performed finite element analysis (FEA) simulations to investigate the effect of the channel geometry on the resistance change of the strain sensor using a commercial software package ABAQUS. The FEA mode of polyimine-LM strain sensor is shown in Figure S7. Figure 3b gives the load-extension curves up to 60 mm elongation (stretched by 150% in horizontal direction), obtained by experiment and FEA, which show good agreement. When uniaxial strain of 100% was applied, the deformed shape of the LM channel and the corresponding contour plot of the

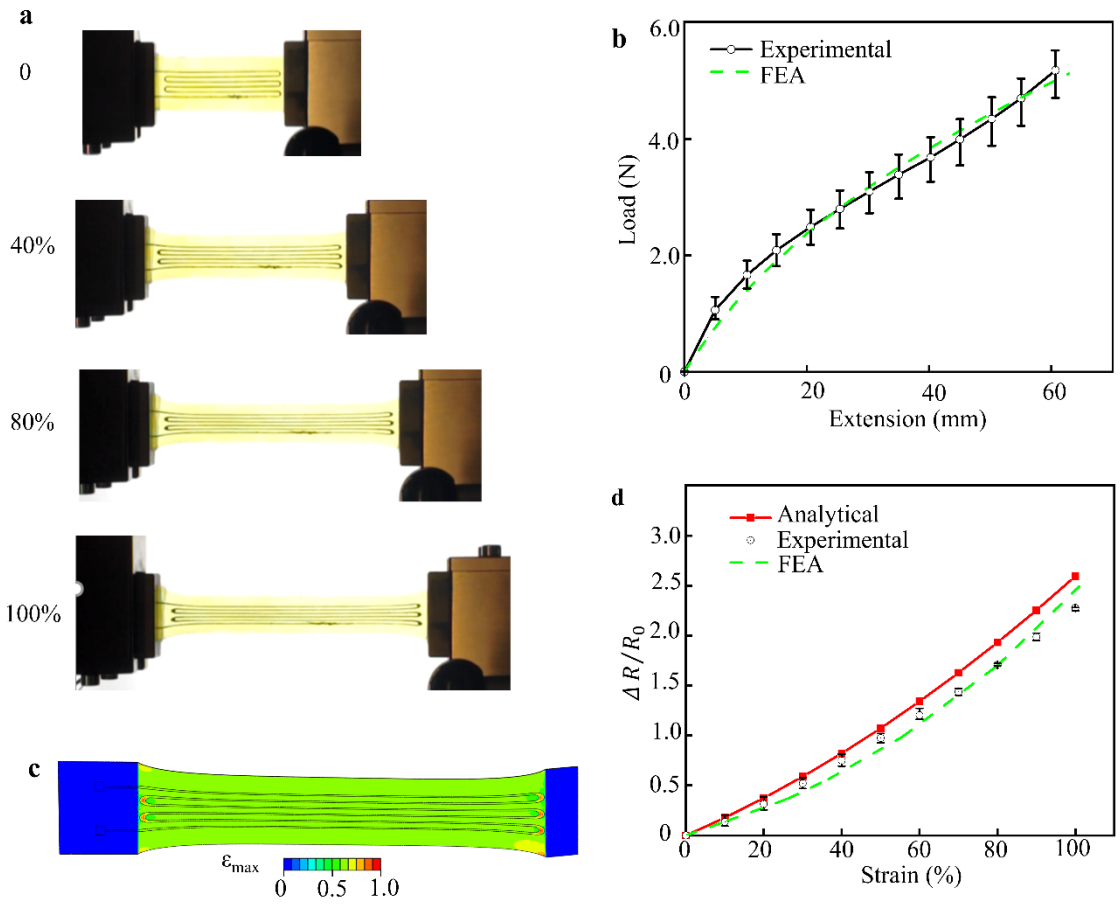

Figure 3. Theoretical and experimental studies of the stretching behavior of a serpentine polyimine-LM strain sensor. (a) Optical images of the serpentine strain sensor at 0%, 40%, 80% and 100% strain. (b) Load-extension curves from experiment and FEA. (c) The max principal strain contour of the serpentine strain sensor when stretched by 100%. (d) Comparison of the fractional change of resistance between experimental, analytical and FEA results.

Inserting Equation (1) to (13), the fractional change in resistance of the serpentine polyimine-LM strain sensor is

max principle strain are shown in Figure 3c. The deformed geometries obtained from the FEA results can be used to

calculate the electrical resistance of the strain sensor. Figure 3d presents the results of fractional change in resistance versus strain ε of the serpentine sensor. The analytical results and FEA simulation results agree well with the experimental resistance change up to 100% strain.

4. Characterization and Performance

Cyclic tensile tests were performed to assess the response of the strain sensor. 100 consecutive cyclic loading to a strain of 40% (the strain of human skin is usually less than 40%[58–60]) and unloading to zero were applied to the serpentine strain sensor under quasi-static condition. Figure 4a (top) shows the fractional resistance change and cyclic strain loading in the first 15 cycles, and it can be seen that the strain sensor shows good recovery. Figure 4a (bottom) shows stable upper and lower envelope values of the resistance of 100 cycles, which demonstrates the robustness of the device. As a result, such strain sensor has good sensing performance. When compared with the recent work of rehealable strain sensors in Figure 4b[61-65], such strain sensor is an excellent candidate in the wearable electronics which combines good sensitivity (GF ~2.27), wide strain range (0~100%), high linearity (R^2~0.993), stable cyclic test (100 cycles), mechanical rehealability (recovery~100%, Figure 5d) and electrical rehealability (recovery~100%, Figure 5c). It's worth pointing out that the strain sensing system has a broad sensing range (Figures 2c and 3d) due to high stretchability, so that such strain sensors can be successfully applied to full-range human activities' monitoring, especially for vigorously joints-related behaviors[66]. As an application in Figure 4c, a serpentine strain sensor was mounted on a knee joint by a VHB double sided tape (3M Company, United States). The knee-mounted sensor reliably detected resistance changes in response to the degree of bending of

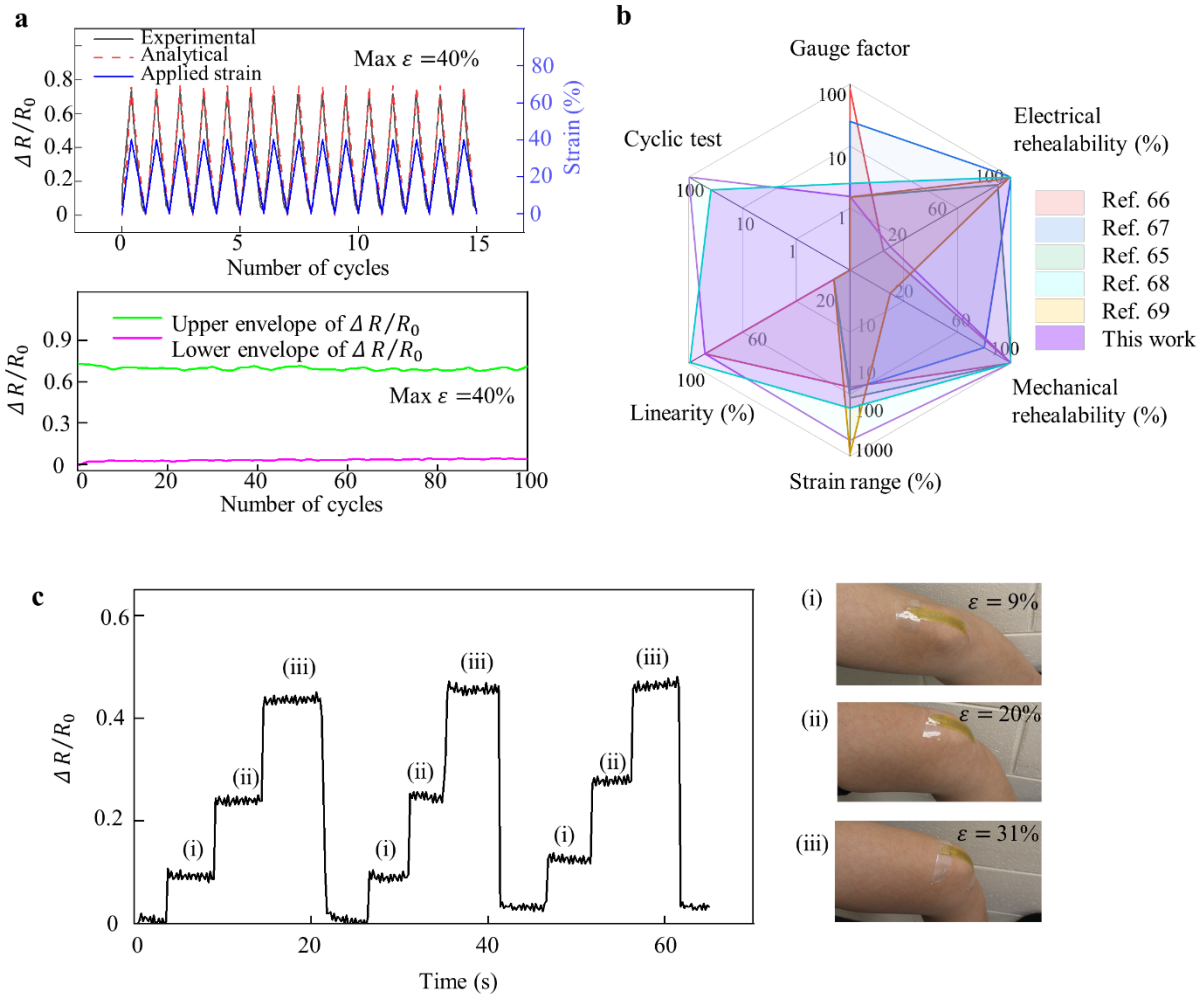

Figure 4. Characterization and application of the serpentine strain sensor. (a) The fractional change of resistance in the first 15 cycles (top) and the envelopes of the resistance change in 100 cycles (bottom) during a cyclic loading test. (b) Comparison of this work with currently reported strain sensors in terms of strain range, gauge factor, cyclic test, linearity, mechanical rehealability and electrical rehealability. (c) The fractional change of resistance at different deformation states of a human joint in real time.

the joint, and thus distinguished different knee motions (Figure 4c, left). The resistance increased rapidly during bending, remained unchanged when the knee was kept flexed, and returned to its original value once the joint was entirely relaxed. The maximum strain occurred when the knee bended by ~90 degrees, and it was measured to be 31%. From Figure 4c, the change of resistance slightly increases with the increasing cyclic time at 9%, 20% and 31% of strain, which is because of the slight hysteresis from polyimine material under cyclic test.

5. Rehealablility of Strain Sensors

In addition to superior electrical and mechanical properties, the wearable strain sensing system also exhibits excellent rehealing capability, which owns to the bond exchange reaction of polyimine matrix and the fluidity of LM conductor. In Figure 5a, the detailed rehealing process of damaged serpentine polyimine-LM strain sensor is schematically illustrated, and the microscope images, where applicable, are placed below the corresponding schematic

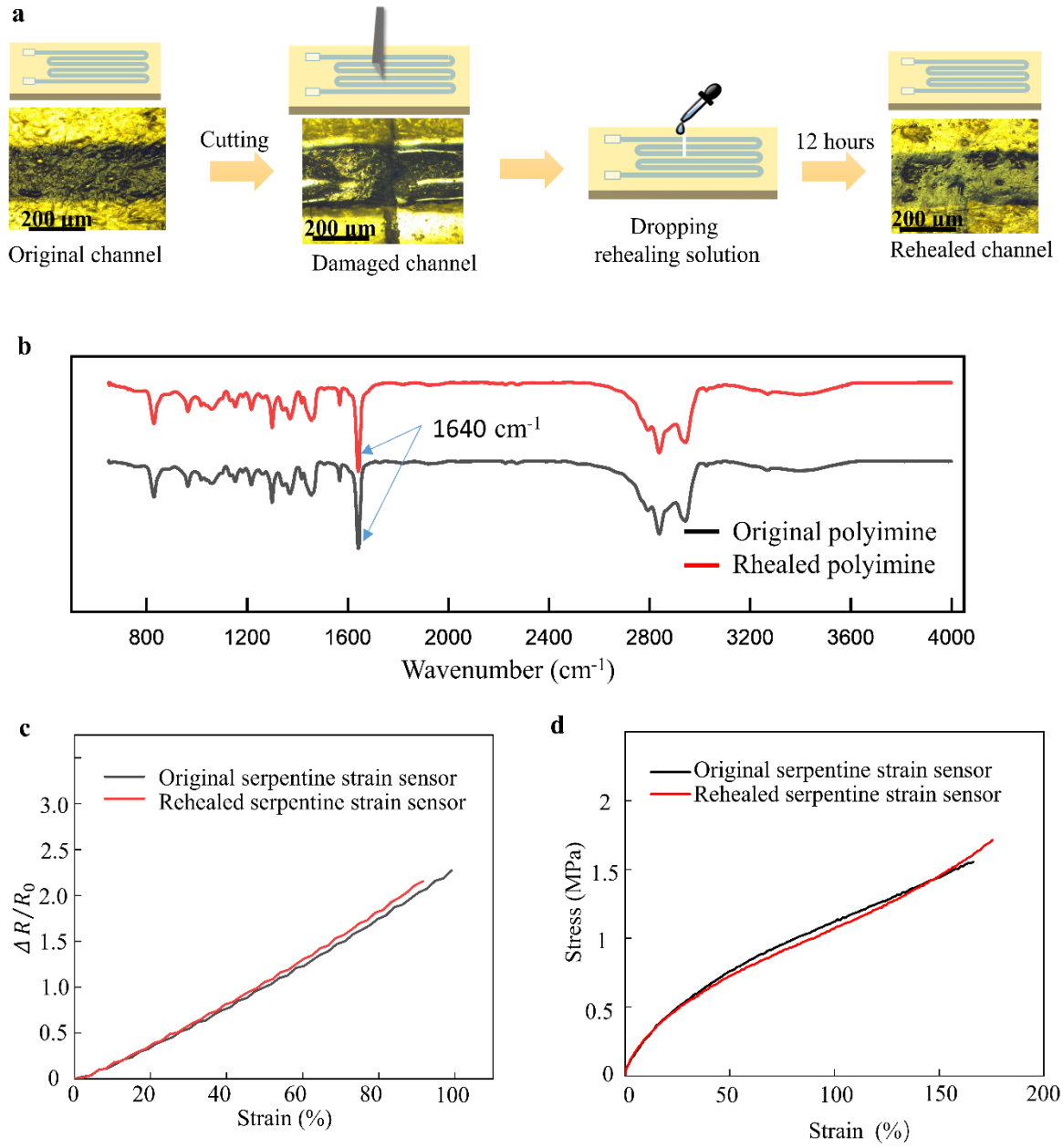

Figure 5. Rehealing of the polyimine-LM strain sensor. (a) Schematic and optical microscope images of the serpentine strain sensor during rehealing process. (b) FTIR of original polyimine (black) and rehealed polyimine (red). Comparison of the fractional change of resistance versus strain (c) and stress-strain curves (d) between the original and rehealed serpentine strain sensors

diagrams. The original channel (Figure 5a, left frame) was cut broken along its width direction (Figure 5a, the second frame). By applying a drop of rehealing solution at the damaged area (Figure 5a, the third frame) and waiting for 12 hours at room temperature, the cut was rehealed and the crack trace disappeared (Figure 5a, the fourth frame). This can be clearly seen from the optical microscopy images: the cut had a width of ~80 μm initially (Figure 5a, the second frame), and became invisible after being rehealed (Figure 5a, the fourth frame). Figure S8 provides the optical images of the rehealing process of a serpentine strain sensor, in which the rehealed strain sensor can be stretched by 100%. It should be noted that the rehealing process in polyimine generates new oligomers/polymers across the broken surfaces based on transamination, which eventually leads to imine bonding (chemical) of the two pieces without existing interfaces at the cut area[49]. As proved in Fig. 5b, the Fourier transform infrared (FTIR) spectra of polyimine films further support that the original and rehealed polyimine are chemically identical. So that, the mechanism of rehealing capability is intrinsically different from the physical glue bonding (van der Waals interactions) at the interface. It's also worth to point that the repair mechanism of LM is more like self-healability, because the LM conductor can connect again due to its fluidity, which doesn't conflict with the rehealing capability of the whole system.

Figure 5c compares the resistance of the rehealed strain sensor with that of the original device during stretching, which states that the sensor has almost identical electrical properties before and after rehealing. The mechanical properties have also been compared between the rehealed sensor and the original device in Figure 5d. The stress-strain curves of the device before and after rehealing are almost identical up to a tensile strain of 170%. It is thus evident that the sensor, which completely loses its functionality after being cut broken, can reheal and regain its full sensing functionality and mechanical integrity that are comparable to the original device.

6. Experimental

6.1 Polyimine synthesis

The polyimine was synthesized by mixing terephthalaldehyde (0.5 g, 3.72 mmol), 3,3′-Diamino-*N*-methyldipropylamine (0.417 g, 2.72 mmol), and tris(2-aminoethyl)amine (0.084 g, 0.57 mmol) in methanol as shown in Figure S1. After vigorously stirring and pouring the solution into a silicone paper mold, the uncured polyimine was cured in a fume hood for 12 hours at room temperature, and cured polyimine film was heat-pressed at 80 ^{0}C and 8.5 kPa for 12 hours.

6.2 SiO_2 LM preparation

Pure LM is a eutectic metal alloy consisting of gallium (75%) and indium (25%) (EGaIn, Sigma-Aldrich), which has a melting point of 15.7°C and a resistivity of only 29.4 × 10^{-6} Ω/cm[30,67]. In order to increase the initial resistivity of LM to improve strain sensitivity, the EGaIn was mixed with 6%wt SiO_2 microparticles (40 μm diameter, Sigma-Aldrich) at room temperature. The mixture was stirred at 500 rpm for 2 minutes and 2000 rpm for 8 minutes. As a result, the doped LM has a resistivity of 95 × 10^{-6} Ω/cm.

6.3 Fabrication and characterization of stain sensor

A 0.2 mm thick silicone paper film (Ruspepa non-stick silicone paper) was cut by a laser cutter (Lide laser cutting machine), laminated over a weakly adhering polyimide film substrate, and doped LM was printed over the sensor mask: a razor blade was swiped across. The LM solidifies after been cooled below 15.7 ℃, and removal of the mask left LM to be printed on the polyimine membrane. Pouring the same formula polyimine solution and curing at low temperature (<15.7 ℃) encapsulated the LM. To connect the device to the external data acquisition equipment, two copper wires were embedded in the polyimine, forming contact with LM.

6.4 Fabrication and characterization of stain sensor

To reheal the polyimine films, a small drop of rehealing agent (the same formula for polyimine solution) was applied to the crack, and allowed for curing for 12 hours at room temperature.

6.5 Tension and cyclic mechanical test

Poyimine-LM strain sensors were tested using an Instron mechanical testing system, under quasi-static tension conditions[68, 69]. The testing strain sensors were prepared in the shape shown in Figure 3a (0.29 mm × 18 mm × 40 mm). Four-point measurement was adopted to measure the resistance change. A current supplier (HY3005M-3 Digital Control) was used for the current input, and Arduino and 16-Bit analog-to-digital converter (ADS1115, Texas Instruments) were used for measuring the voltage every 0.1 seconds. A constant current of 10 mA was applied on the strain sensors.

7. Conclusions

A highly stretchable and rehealable wearable strain sensor with a wide sensing range is presented in the article. The integrated sensor is fabricated by encapsulating LM in a dynamic covalent thermoset polyimine matrix through a low-cost process. The combination of conductive and deformable LM with compliant polymine matrix assures reliable sensing performance of the strain sensor even at large strain (up to 100%). An analytical model has been developed to predict the fractional change of resistance with the applied strain,

and it agrees well with FEA and experimental results. Moreover, cyclic loading/unloading tests show that the strain sensor performs reliably even up to 100 cycles. Furthermore, the device can also reheal perfectly from damages, which is enabled by the bond exchange reactions in the polyimine network and flowability of the LM conductor. Finally, to demonstrate applicability, a wearable strain sensor has been designed and mounted on the knee joint. Experimental results show that it can precisely identify the physical motion states of the joint. The superior properties make the polyimine-LM strain sensor quantitatively precise, economically friendly and environmentally sustainable, and thus can find wide applications in robotics, health care, prosthetics and virtual reality.

Acknowledgements

This work was supported by National Science Foundation of China (Project No. 11972259), Shanghai Sailing Program (Project No. 20YF1452300), and National Science Foundation (CMMI-1762324).

C. Shi, Y. Zhao performed the analysis. C. Shi, P. Zhu and J. Xiao designed the experiments. C. Shi, Y. Zhao, J. Xiao and G.H. Nie wrote the paper. G.H. Nie initiated the paper. All authors have given approval to the final version of the manuscript.

The authors declare that they have no known competing financial interests or personal relationships that could have appeared to influence the work reported in this paper.

References

[1] Kim D-H, Ahn J-H, Choi W M, Kim H-S, Kim T-H, Song J, Huang Y Y, Liu Z, Lu C and Rogers J A 2008 Stretchable and Foldable Silicon Integrated Circuits *Science.* **320** 507–11

[2] Sekitani T, Yokota T, Zschieschang U, Klauk H, Bauer S, Takeuchi K, Takamiya M, Sakurai T and Someya T 2009 Organic Nonvolatile Memory Transistors for Flexible Sensor Arrays *Science.* **326** 1516–9

[3] Song Y M, Xie Y, Malyarchuk V, Xiao J, Jung I, Choi K-J, Liu Z, Park H, Lu C, Kim R-H, Li R, Crozier K B, Huang Y and Rogers J A 2013 Digital cameras with designs inspired by the arthropod eye *Nature* **497** 95–9

[4] Gao W, Emaminejad S, Nyein H Y Y, Challa S, Chen K, Peck A, Fahad H M, Ota H, Shiraki H, Kiriya D, Lien D-H, Brooks G A, Davis R W and Javey A 2016 Fully integrated wearable sensor arrays for multiplexed in situ perspiration analysis *Nature* **529** 509–14

[5] Qiu Y, Tian Y, Sun S, Hu J, Wang Y, Zhang Z, Liu A, Cheng H, Gao W, Zhang W, Chai H and Wu H 2020 Bioinspired, multifunctional dual-mode pressure sensors as electronic skin for decoding complex loading processes and human motions *Nano Energy* **78** 105337

[6] Qiu Y, Sun S, Xu C, Wang Y, Tian Y, Liu A, Hou X, Chai H, Zhang Z and Wu H 2021 The frequency-response behaviour of flexible piezoelectric devices for detecting the magnitude and loading rate of stimuli *J. Mater. Chem. C* **9** 584–94

[7] Minev I R, Musienko P, Hirsch A, Barraud Q, Wenger N, Moraud E M, Gandar J, Capogrosso M, Milekovic T, Asboth L, Torres R F, Vachicouras N, Liu Q, Pavlova N, Duis S, Larmagnac A, Vörös J, Micera S, Suo Z, Courtine G and Lacour S P 2015 Electronic dura mater for long-term multimodal neural interfaces *Science.* **347** 159–63

[8] Kim D-H, Lu N, Ma R, Kim Y-S, Kim R-H, Wang S, Wu J, Won S M, Tao H, Islam A, Yu K J, Kim T, Chowdhury R, Ying M, Xu L, Li M, Chung H-J, Keum H, McCormick M, Liu P, Zhang Y-W, Omenetto F G, Huang Y, Coleman T and Rogers J A 2011 Epidermal Electronics *Science.* **333** 838–43

[9] Kim D-H, Viventi J, Amsden J J, Xiao J, Vigeland L, Kim Y S, Blanco J A, Panilaitis B, Frechette E S, Contreras D, Kaplan D L, Omenetto F G, Huang Y, Hwang K-C, Zakin M R, Litt B and Rogers J A 2010 Dissolvable films of silk fibroin for ultrathin conformal bio-integrated electronics *Nat. Mater.* **9** 511–7

[10] Rogers J A, Someya T and Huang Y 2010 Materials and mechanics for stretchable electronics *Science.* **327** 1603–7

[11] Bilodeau R A, Mohammadi Nasab A, Shah D S and Kramer-Bottiglio R 2020 Uniform conductivity in stretchable silicones: Via multiphase inclusions *Soft Matter* **16** 5827–39

[12] Zhang Y, Xu S, Fu H, Lee J, Su J, Hwang K C, Rogers J A and Huang Y 2013 Buckling in serpentine microstructures and applications in elastomer-supported ultra-stretchable electronics with high areal coverage *Soft Matter* **9** 8062–70

[13] Kim D H, Song J, Choi W M, Kim H S, Kim R H, Liu Z, Huang Y Y, Hwang K C, Zhang Y W and Rogers J A 2008 Materials and noncoplanar mesh designs for integrated circuits with linear elastic responses to extreme mechanical deformations *Proc. Natl. Acad. Sci. U. S. A.* **105** 18675–80

[14] Someya T, Kato Y, Sekitani T, Iba S, Noguchi Y, Murase Y, Kawaguchi H and Sakurai T 2005 Conformable, flexible, large-area networks of pressure and thermal sensors with organic transistor active matrixes *Proc. Natl. Acad. Sci. U. S. A.* **102** 12321–5

[15] Kim K S, Zhao Y, Jang H, Lee S Y, Kim J M, Kim K S, Ahn J H, Kim P, Choi J Y and Hong B H 2009 Large-scale pattern growth of graphene films for stretchable transparent electrodes *Nature* **457** 706–10

[16] Lee S, Sasaki D, Kim D, Mori M, Yokota T, Lee H, Park S, Fukuda K, Sekino M, Matsuura K, Shimizu T and Someya T 2019 Ultrasoft electronics to monitor dynamically pulsing cardiomyocytes *Nat. Nanotechnol.* **14** 156–60

[17] Sekitani T, Noguchi Y, Hata K, Fukushima T, Aida T and Someya T 2008 A Rubberlike Stretchable Active Matrix Using Elastic Conductors *Science.* **321** 1468–73

[18] Siegel A C, Bruzewicz D A, Weibel D B and Whitesides G M 2007 Microsolidics: Fabrication of three-dimensional metallic microstructures in poly(dimethylsiloxane) *Adv. Mater.* **19** 727–33

[19] Guo C F, Liu Q, Wang G, Wang Y, Shi Z, Suo Z, Chu C W and Ren Z 2015 Fatigue-free, superstretchable, transparent, and biocompatible metal electrodes *Proc. Natl. Acad. Sci. U. S. A.* **112** 12332–7

[20] Lukáš P, Klesnil M and Polák，J 1974 High cycle fatigue life of metals *Mater. Sci. Eng.* **15** 239–45

[21] Lipomi D J, Vosgueritchian M, Tee B C K, Hellstrom S L, Lee J A, Fox C H and Bao Z 2011 Skin-like pressure and strain sensors based on transparent elastic films of carbon nanotubes *Nat. Nanotechnol.* **6** 788–92

[22] Yamada T, Hayamizu Y, Yamamoto Y, Yomogida Y, Izadi-najafabadi A, Futaba D N and Hata K 2011 A stretchable carbon nanotube strain sensor for human-motion detection *Nat. Nanotechnol.* **6** 296–301

[23] Li Y, Miao X, Chen J Y, Jiang G and Liu Q 2020 Sensing performance of knitted strain sensor on two-dimensional and three-dimensional surfaces *Mater. Des.* **197** 109273

[24] Xia S, Song S, Jia F and Gao G 2019 Flexible, Adhesive and Self-Healable Hydrogel-based Wearable Strain Sensor for Human Motion and Physiological Signal Monitoring *J. Mater. Chem. B* **7** 4638–48

[25] Choi S and Kang S 2018 Monitoring rehabilitation with transient sensors *Nat. Electron.* **1** 272–3

[26] Li Y, Liu C, Lv X and Sun S 2021 A highly sensitive strain sensor based on a silica@polyaniline core–shell particle reinforced hydrogel with excellent flexibility, stretchability, toughness and conductivity *Soft Matter*

[27] Li Z, Meng X, Xu W, Zhang S, Ouyang J, Zhang Z, Liu Y, Niu Y, Ma S, Xue Z, Song A, Zhang S and Ren C 2020 Single network double cross-linker (SNDCL) hydrogels with excellent stretchability, self-recovery, adhesion strength, and conductivity for human motion monitoring *Soft Matter* **16** 7323–31

[28] Wang S, Zhang X, Wu X and Lu C 2016 Tailoring percolating conductive networks of natural rubber composites for flexible strain sensors via a cellulose nanocrystal templated assembly *Soft Matter* **12** 845–52

[29] Amjadi M, Turan M, Clementson C P and Sitti M 2016 Parallel Microcracks-based Ultrasensitive and Highly Stretchable Strain Sensors *ACS Appl. Mater. Interfaces* **8** 5618–26

[30] Chossat J, Park Y, Wood R J and Duchaine V 2013 A Soft Strain Sensor Based on Ionic and Metal Liquids *IEEE Sens. J.* **13** 3405–14

[31] Obitayo W and Liu T 2015 Effect of orientation on the piezoresistivity of mechanically drawn single walled carbon nanotube (SWCNT) thin films *Carbon N. Y.* **85** 372–82

[32] Zhong J, Zhang Y, Zhong Q, Hu Q, Hu B, Wang Z L and Zhou J 2014 Fiber-based generator for wearable electronics and mobile medication *ACS Nano* **8** 6273–80

[33] Toohey K S, Sottos N R, Lewis J A, Moore J S and White S R 2007 Self-healing materials with microvascular networks *Nat. Mater.* **6** 581–5

[34] Adzima B J, Kloxin C J and Bowman C N 2010 Externally Triggered Healing of a Thermoreversible Covalent Network via Self-Limited Hysteresis Heating *Adv. Mater.* **22** 2784–7

[35] Tee B C K, Wang C, Allen R and Bao Z 2012 An electrically and mechanically self-healing composite with pressure- and flexion-sensitive properties for electronic skin applications *Nat. Nanotechnol.* **7** 825–32

[36] Oh J Y, Rondeau-Gagné S, Chiu Y C, Chortos A, Lissel F, Wang G J N, Schroeder B C, Kurosawa T, Lopez J, Katsumata T, Xu J, Zhu C, Gu X, Bae W G, Kim Y, Jin L, Chung J W, Tok J B H and Bao Z 2016 Intrinsically stretchable and healable semiconducting polymer for organic transistors *Nature* **539** 411–5

[37] Shi Y, Wang M, Ma C, Wang Y, Li X and Yu G 2015 A Conductive Self-Healing Hybrid Gel Enabled by Metal-Ligand Supramolecule and Nanostructured Conductive Polymer *Nano Lett.* **15** 6276–81

[38] Jin Y, Yu C, Denman R J and Zhang W 2013 Recent advances in dynamic covalent chemistry *Chem. Soc. Rev.* **42** 6634–54

[39] Taynton P, Ni H, Zhu C, Yu K, Loob S, Jin Y, Qi H J and Zhang W 2016 Repairable Woven Carbon Fiber Composites with Full Recyclability Enabled by Malleable Polyimine Networks *Adv. Mater.* **28** 2904–9

[40] Taynton P, Yu K, Shoemaker R K, Jin Y, Qi H J and Zhang W 2014 Heat- or Water-Driven Malleability in a Highly Recyclable Covalent Network Polymer *Adv. Mater.* **26** 3938–42

[41] Zou Z, Zhu C, Li Y, Lei X, Zhang W and Xiao J 2018 Rehealable, fully recyclable, and malleable electronic skin enabled by dynamic covalent thermoset nanocomposite *Sci. Adv.* **4** eaaq0508

[42] Dickey M D 2017 Stretchable and Soft Electronics using Liquid Metals *Adv. Mater.* **29** 1–19

[43] Pineda F, Bottausci F, Icard B, Malaquin L and Fouillet Y 2015 Using electrofluidic devices as hyper-elastic strain sensors: Experimental and theoretical analysis *Microelectron. Eng.* **144** 27–31

[44] Matsuzaki R and Tabayashi K 2015 Highly Stretchable, Global, and Distributed Local Strain Sensing Line Using GaInSn Electrodes for Wearable Electronics *Adv. Funct. Mater.* **25** 3806–13

[45] Son D, Kang J, Vardoulis O, Kim Y, Matsuhisa N, Oh J Y, To J W F, Mun J, Katsumata T, Liu Y, Mcguire A F, Krason M, Molina-lopez F, Ham J, Kraft U, Lee Y, Yun Y, Tok J B and Bao Z 2018 An integrated self-healable electronic skin system fabricated via dynamic

reconstruction of a nanostructured conducting network *Nat. Nanotechnol.*

[46] Zeng C, Seino H, Ren J, Hatanaka K and Yoshie N 2013 Bio-Based Furan Polymers with Self-Healing Ability *Macromolecules* **46** 1794–802

[47] Ghosh B and Urban M W 2009 Self-Repairing Oxetane-Substituted Chitosan Polyurethane Networks *Science.* **323** 1458–60

[48] Taynton P, Zhu C, Loob S, Shoemaker R, Pritchard J, Jin Y and Zhang W 2016 Re-healable polyimine thermosets: Polymer composition and moisture sensitivity *Polym. Chem.* **7** 7052–6

[49] Chen X, Dam M A, Ono K, Mal A, Shen H, Nutt S R, Sheran K and Wudl F 2002 A thermally re-mendable cross-linked polymeric material *Science.* **295** 1698–702

[50] Jin Y, Lei Z, Taynton P, Huang S and Zhang W 2019 Malleable and Recyclable Thermosets : The Next Generation of Plastics *Matter* **1** 1456–93

[51] Shi C, Zou Z, Lei Z, Wu X, Liu Z, Lu H, Zhang W and Xiao J 2019 Investigating the Self-Healing of Dynamic Covalent Thermoset Polyimine and Its Nanocomposites *J. Appl. Mech. Trans. ASME* **86** 1–6

[52] Yao S and Zhu Y 2014 Wearable multifunctional sensors using printed stretchable conductors made of silver nanowires *Nanoscale* **6** 2345–52

[53] Liu X, Lu C, Wu X and Zhang X 2017 Self-healing strain sensors based on nanostructured supramolecular conductive elastomers *J. Mater. Chem. A* **5** 9824–32

[54] Shi C, Zou Z, Lei Z, Zhu P, Zhang W and Xiao J 2020 Heterogeneous integration of rigid, soft, and liquid materials for self-healable, recyclable, and reconfigurable wearable electronics *Sci. Adv.* **6** 1–9

[55] Lu N, Lu C, Yang S and Rogers J 2012 Highly sensitive skin-mountable strain gauges based entirely on elastomers *Adv. Funct. Mater.* **22** 4044–50

[56] Hafeez H, Shi C, Lee C M, Periyanayagam J J, Kim D H, Song M, Kim C S, Zou Z, Xiao J and Ryu S Y 2019 Improved design of highly efficient microsized lithium-ion batteries for stretchable electronics *J. Micromechanics Microengineering* **29** 075008

[57] Wu Y H, Zhen R M, Liu H Z, Liu S Q, Deng Z F, Wang P P, Chen S and Liu L 2017 Liquid metal fiber composed of a tubular channel as a high-performance strain sensor *J. Mater. Chem. C* **5** 12483–91

[58] Soomro A M, Khalid M A U, Shah I, Kim S W, Kim Y S and Choi K H 2020 Highly stable soft strain sensor based on Gly-KCl filled sinusoidal fluidic channel for wearable and water-proof robotic applications *Smart Mater. Struct.* **29** 1–15

[59] Hirsch A, Michaud H O, Gerratt A P, de Mulatier S and Lacour S P 2016 Intrinsically Stretchable Biphasic (Solid–Liquid) Thin Metal Films *Adv. Mater.* **28** 4507–12

[60] Yao S, Swetha P and Zhu Y 2018 Nanomaterial-Enabled Wearable Sensors for Healthcare *Adv. Healthc. Mater.* **7** 1700889

[61] Wessendorf A M and Newman D J 2012 Dynamic understanding of human-skin movement and strain-field analysis *IEEE Trans. Biomed. Eng.* **59** 3432–8

[62] Jiang D, Wang Y, Li B, Sun C, Wu Z, Yan H, Xing L, Qi S, Li Y, Liu H, Xie W, Wang X, Ding T and Guo Z 2019 Flexible Sandwich Structural Strain Sensor Based on Silver Nanowires Decorated with Self-Healing Substrate *Macromol. Mater. Eng.* **304** 1900074

[63] Cai G, Wang J, Qian K, Chen J, Li S and Lee P S 2017 Extremely Stretchable Strain Sensors Based on Conductive Self-Healing Dynamic Cross-Links Hydrogels for Human-Motion Detection *Adv. Sci.* **4** 1600190

[64] Huynh T and Haick H 2016 Self-Healing , Fully Functional , and Multiparametric Flexible Sensing Platform *Adv. Mater.* **28** 138–43

[65] Xu J, Wang Z, You J, Li X, Li M, Wu X and Li C 2020 Polymerization of moldable self-healing hydrogel with liquid metal nanodroplets for flexible strain-sensing devices *Chem. Eng. J.* **392** 123788

[66] Li Y, He T, Shi L, Wang R and Sun J 2020 Strain Sensor with Both a Wide Sensing Range and High Sensitivity Based on Braided Graphene Belts *ACS Appl. Mater. Interfaces* **12** 17691–8

[67] Dickey M D, Chiechi R C, Larsen R J, Weiss E A, Weitz D A and Whitesides G M 2008 Eutectic Gallium-Indium (EGaIn): A Liquid Metal Alloy for the Formation of Stable Structures in Microchannels at Room Temperature *Adv. Funct. Mater.* **18** 1097–104

[68] W. Grellmann, S. Seidler, Mechanical Properties of Polymers in *Polymer Testin*, Seidler, Hanser, Munich, 2007.

[69] Standard Test Method for Tensile Properties of Plastics. *ASTM D638 – 10*, 2010. https://doi.org/10.1520/D0638-10

Supporting Information

Highly Stretchable and Rehealable Wearable Strain Sensor Based on Dynamic Covalent Thermoset and Liquid Metal

Chuanqian Shi[1,2,†], Ying Zhao[1,†] Pengcheng Zhu[2,3] Jianliang Xiao[2,*] and Guohua Nie[1,*]

[1] School of Aerospace Engineering and Applied Mechanics, Tongji University, Shanghai 200092, China
[2] Department of Mechanical Engineering, University of Colorado Boulder, Boulder, Colorado 80309, USA
[3] School of Physics and Microelectronics, Zhengzhou University, Zhengzhou 450001, China.
† These authors contributed equally.
E-mail: ghnie@tongji.edu.cn (G.H. Nie), Jianliang.Xiao@colorado.edu (J. Xiao)

1. Supplementary text

FEA simulation: To investigate the influence of mechanical deformation for resistance change of the strain sensors, finite element analysis (FEA) was conducted using a commercial software package ABAQUS. The loading and boundary conditions in FEA are the same as to the experiments, which is given in Figure 3a. The polyimine and LM were modeled as hyperelastic material using 3D hybrid stress elements (C3D8H). A Yeoh hyperelastic material model was used to take into account the nonlinear stress-strain relation of the polyimine films under large deformation. In the Yeoh model, the strain energy density for incompressible model is written as[1]

$$W = \sum_{i=1}^{3} C_i (I_1 - 3)^i \qquad (S1)$$

where C_i are the material coefficients. To acquire the Yeoh material parameters of polyimine, we conducted uniaxial tensile tests using a dumbbell specimen as shown in Fig. S2. With the experimental data plotted in Fig. S3, a least-squares fit of the stress−strain equations were

$C_1 = 0.457$, $C_2 = -0.025$, $C_3 = 0.001$. LM conductors were modeled as an Neo-Hookean hyperelastic material model. Because the shear modulus of LM measured by rheometer was ~1 kPa, the parameter of LM of Neo-Hookean model is $C_{10} = 0.0005$. Figure S5 (top) shows an undeformed polyimine-LM strain sensor FEA model.

2. Supplementary Figure Captions

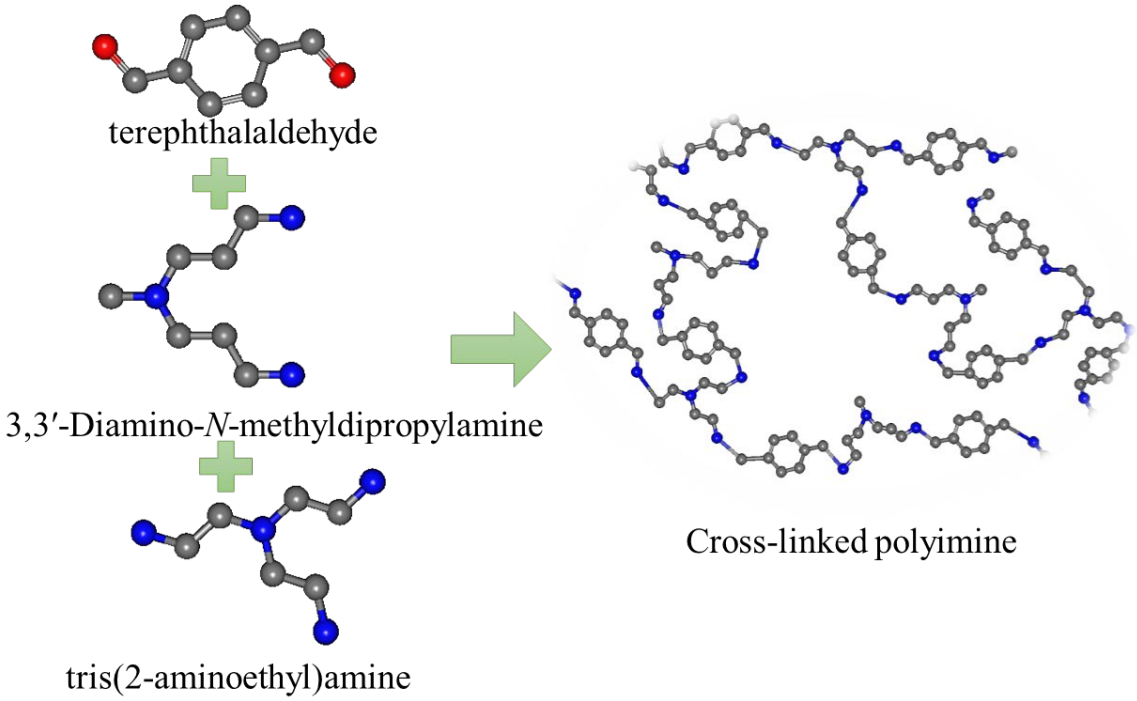

Figure S1. Polymerization of polyimine.

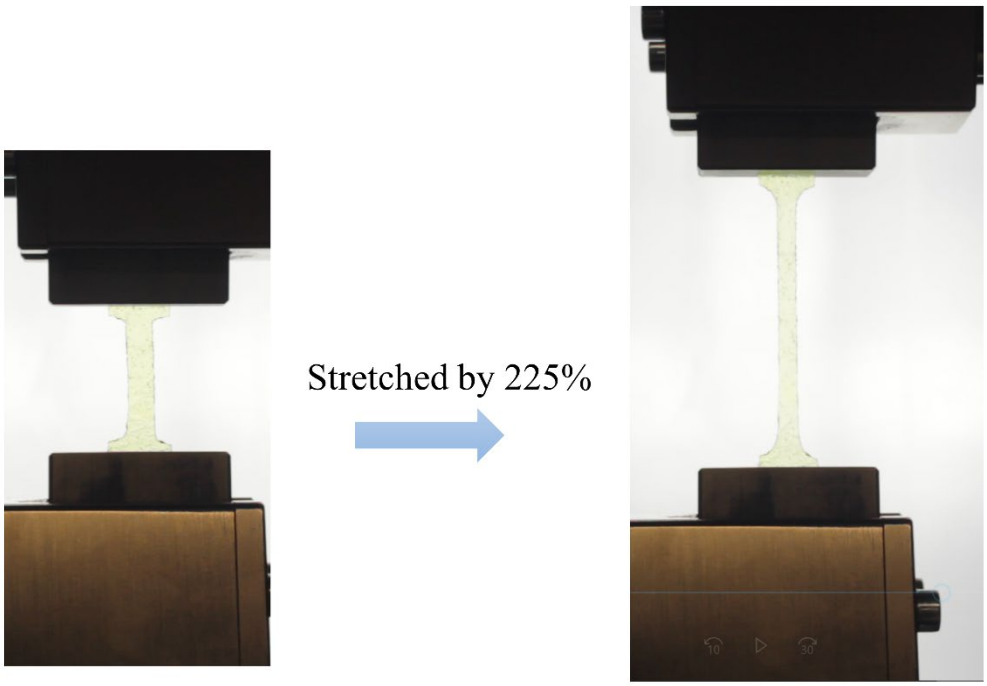

Figure S2. Optical images of the polyimine sample(left) uniaxial stretched by 225%(right).

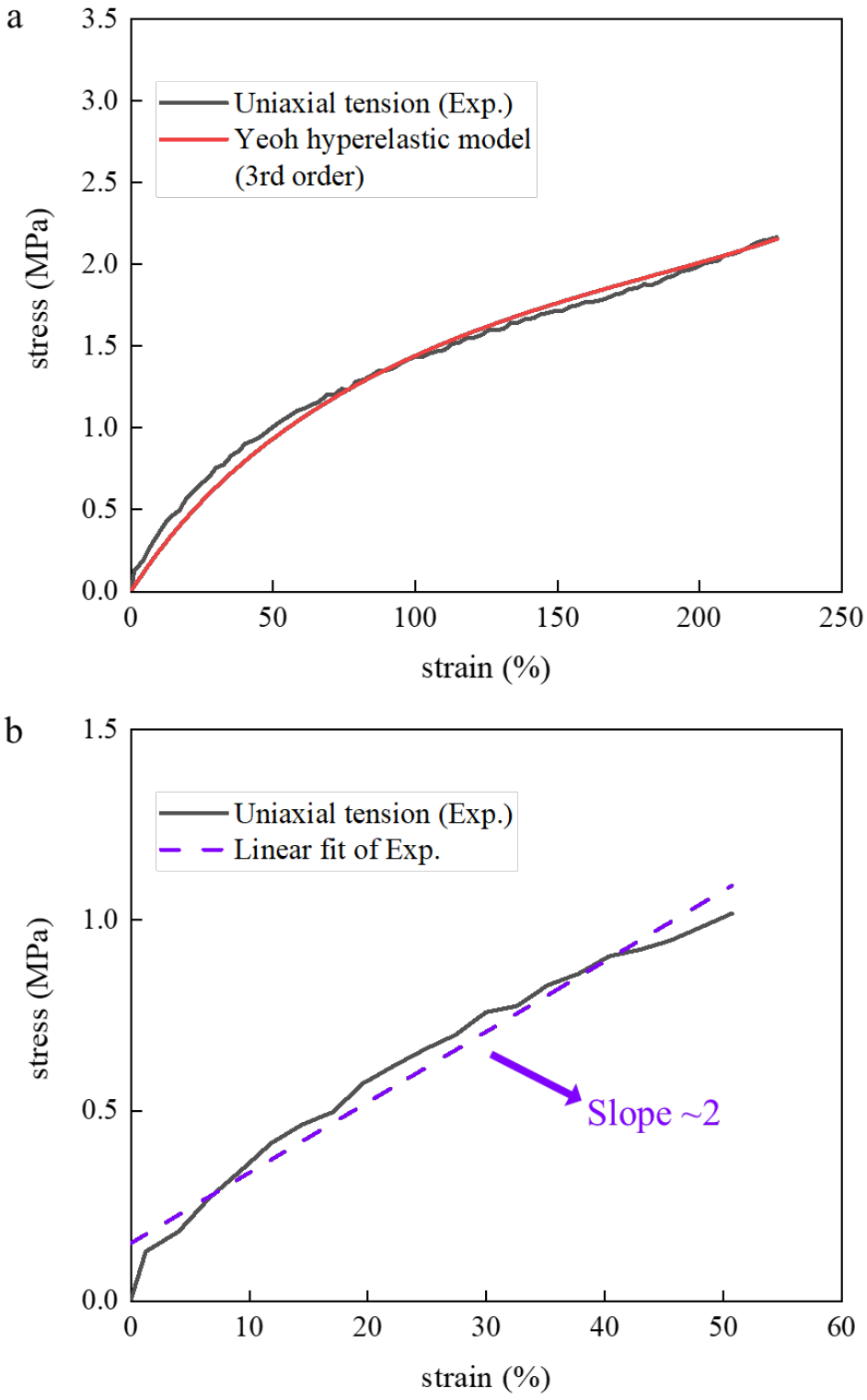

Figure S3. Stress-strain curve obtained by Yeoh hyperelastic material model fit to the data from a uniaxial tensile testing(a), and the linear fitting at small strain (b).

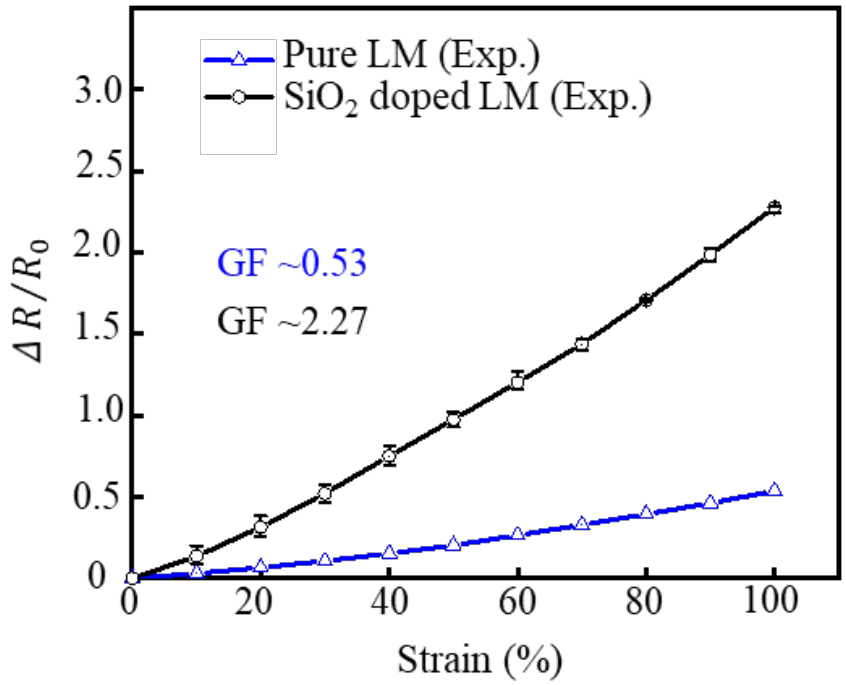

Figure S4. The comparision of GF between pure LM and SiO_2 doped LM

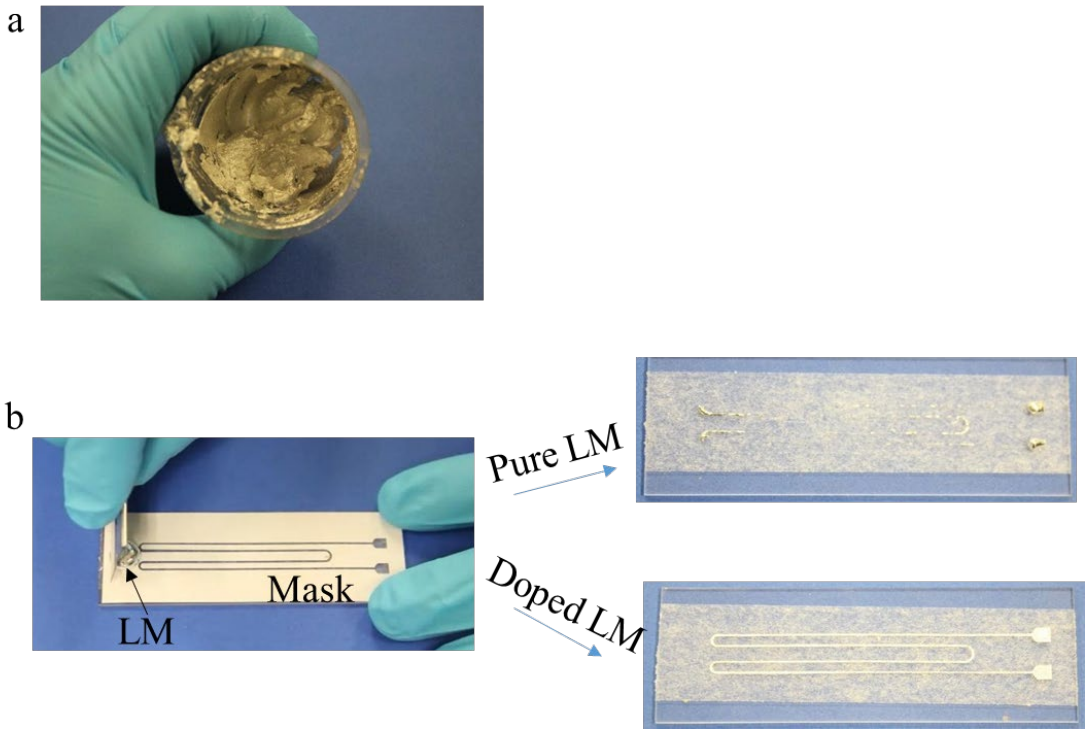

Figure S5. (a) The optical image of doped LM mixed with SiO_2. (b) The optical images about printing LM over the mask (left), the fragmentary printed patterns of pure LM (top right), and the complete printed patterns of doped LM (bottom right).

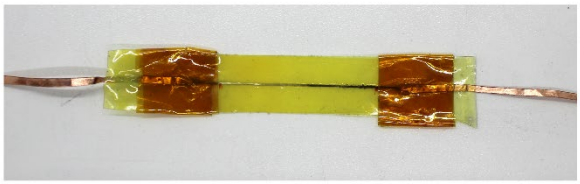

Single-line strain sensor

Stretched by 100%

Figure S6. The optical images of single-line strain sensors(top) and specimens(bottom) can be stretched by 100%.

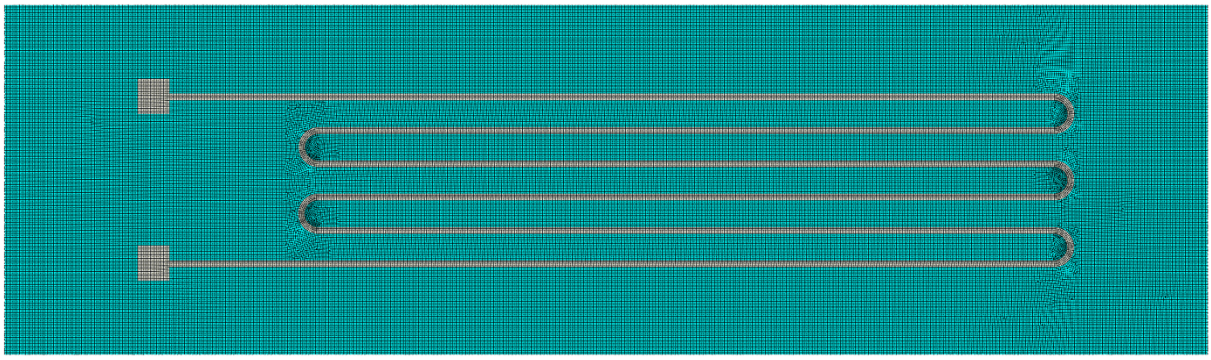

Figure S7. FEA model of the serpentine strain sensor.

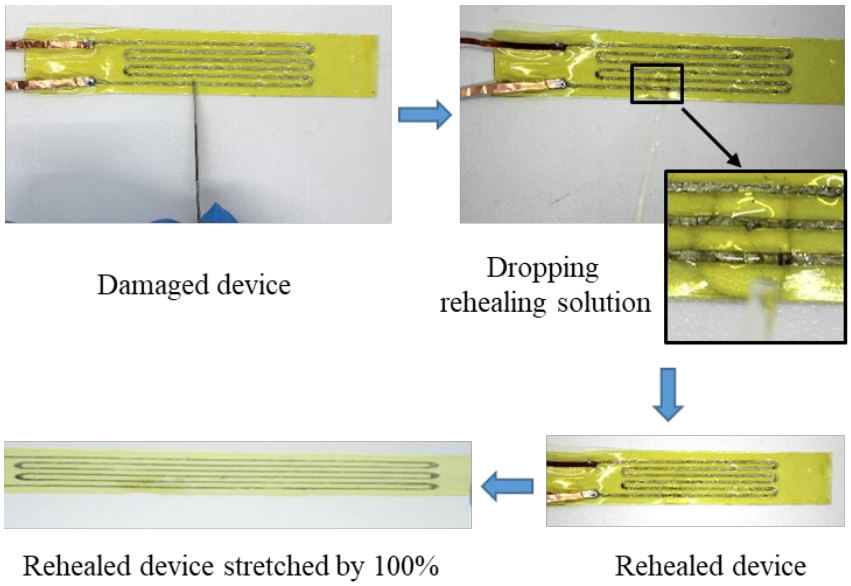

Figure S8. The optical images of the rehealing process of a serpentine strain sensor.

References

1 K. Estelle, D. Blair, K. Evans and B. A. Gozen, *J. Manuf. Process.*, 2017, **28**, 500–507.